

**Turbulence modulation in non-uniform open-channel clay suspension flows**

**M.G.W. de Vet<sup>1</sup>, R. Fernández<sup>1</sup>, J.H. Baas<sup>2</sup>, W.D. McCaffrey<sup>3</sup> and R. M. Dorrell<sup>1</sup>**

<sup>1</sup> Energy and Environment Institute, University of Hull. Hull HU6 7RX, U.K.

<sup>2</sup> School of Ocean Sciences, Bangor University, Menai Bridge, Anglesey LL59 5AB, U.K.

<sup>3</sup> School of Earth and Environment, University of Leeds, Leeds LS2 9 JT, U.K.

Corresponding author: Marijke de Vet (M.G.de-Vet-2018@hull.ac.uk)

**Key Points:**

- Accelerating clay-laden flows adapt faster to velocity changes than decelerating flows; breaking clay bonds is easier than establishing them
- Adaptation timescales grow with clay concentration for decelerating clay-laden flows passing through a larger variety of clay flow types
- Erosional and depositional processes after velocity changes in fluvial or submarine settings are likely to reflect the different timescales

## Abstract

Cohesive properties of clay promote the formation of clay flocs and gels and relatively small suspended clay concentrations can enhance or suppress turbulence in a flow. Flows are naturally non-uniform, varying in space and time, yet the dynamics of non-uniform open-channel clay suspension flows are poorly understood. To research the influence of suspended cohesive clay on changing flow dynamics under non-uniform flow conditions, new experiments were conducted using decelerating and accelerating clay suspension open-channel flows in a recirculating flume. The flows transition between clay flow types, with different degrees of turbulence enhancement and attenuation as the flow adapts to the change in velocity. The experimental results show that decelerating clay suspension flows have a longer adaptation time than accelerating clay suspension flows. The formation of bonds between cohesive sediment particles is a time-dependent process and establishing clay bonds, as in the decelerating flows, requires more time than breaking them, as in the accelerating flows. This hysteresis is more pronounced for higher concentration decelerating flows that pass through a larger variety of flow phases of turbulence enhancement and attenuation. These different adaptation time scales and associated clay flow type transitions are likely to affect erosional and depositional processes in a variety of fluvial and submarine settings.

## Plain Language Summary

Flows in natural environments, such as rivers, estuaries, seas and oceans, can transport sediment in suspension. The suspended sediment can increase or decrease turbulence within a flow, depending on the sediment concentration. Clay has the ability to form bonds between the individual particles and therefore even small concentrations are sufficient to alter turbulence levels within a flow. The amount of alteration of turbulence is known for uniform, constant flow conditions, but in natural environments, flows are often non-uniform. For example, flow variations can occur due to changes in river width or bed slope. The influence of these variations on clay suspension flows is unknown. New physical experiments are conducted where clay suspension flows are decelerated and accelerated. As the flow decelerates, turbulence in the flow is reduced and bonds between the suspended clay particles are established. Turbulence increases as the flow accelerates and clay bonds are broken. Decelerating flow requires more time to adjust to changes in velocity than accelerating flow, as establishing the bonds between clay particles requires more time than breaking them. This means that especially for the decelerating flows, the influence of a change in velocity is noticeable further downstream.

## 1 Introduction

Cohesive sediment-laden flows are important in a wide range of natural environments, such as rivers, estuaries, shallow seas and deep oceans (Whitehouse et al., 2000; Winterwerp and van Kesteren, 2004), and in industrial settings (Ackers et al., 2001). For example, cohesive sediment supply to rivers can be increased by high-magnitude, low-frequency events, such as storms, floods and post-wildfire erosion (Swanson, 1981; Sankey et al., 2017), which occur more often because of climate change (Geertsema et al., 2006; Reneau et al., 2007; Barbero et al., 2015). Further, cohesive sediment is common in submarine gravity currents, such as turbidity currents, hybrid event beds, mass transport events and associated deposits (Talling et al., 2012). The increases in sediment transport can have major impacts on water quality and aquatic ecosystems, including fish habitats, and also on channel morphology (Smith et al., 2011). High suspended

sediment concentrations modify flow dynamics by either enhancing (Best et al., 1997) or dampening turbulence (Bagnold, 1954; Wang and Larsen, 1994), influencing sediment transport rates and erosion and deposition patterns (Partheniades, 1965; Metha et al., 1989). These processes can be enhanced by the presence of cohesive sediment in suspension (Baas and Best, 2002).

Cohesive clay particles may collide and form larger particles, or flocs, when the distance between the particles is sufficiently small (Van Olphen, 1977; Winterwerp and van Kesteren, 2004). Networks of flocs in the flow, i.e., clay gels, enhance viscosity and yield stress, and thus are a key control on flow turbulence (Baas and Best, 2002). Research into steady, uniform clay flows indicate a close interaction between turbulent and cohesive forces, controlling the dynamic structure of clay flows (Baas and Best, 2002; Baas et al., 2009). As the clay concentration increases, it becomes increasingly difficult to break up the cohesive bonds between particles, resulting in the formation of a pervasive network of permanently interlinked clay particles; turbulent energy is dissipated by the high effective viscosity, and the flow becomes laminar. Conversely, the electrostatic bonds between the clay particles can be broken in regions of high shear. Thus, an increase in turbulence generation in the flows by, for example, an increasing flow velocity has the potential to break up bonds between the clay particles and reduce the flow viscosity (Partheniades, 2009). This shifting balance between turbulent and cohesive forces regulates the dynamic structure of cohesive flows (Baas et al., 2009).

Baas et al. (2009) defined a clay flow classification scheme, consisting of five different flow phases in order of increasing clay concentration: turbulent flow, turbulence-enhanced transitional flow, lower transitional plug flow, upper transitional plug flow, and quasi-laminar plug flow (Fig. 1). Turbulent flow has the characteristics of a turbulent, wall-bounded shear flow (Nezu and Nakagawa, 1993) and it exhibits a logarithmic velocity profile with an associated decrease in turbulence intensity away from the bed. The velocity of turbulence-enhanced transitional flows progressively diminishes, in particular close to the base of the flow, accompanied by a progressive increase in turbulence intensity over the full flow depth, whilst the logarithmic velocity profile is maintained. A progressive increase in clay concentration in lower transitional plug flows results in the formation of a plug, which thickens from the water surface downwards. This flow type exhibits a decreased near-bed velocity and increased near-bed turbulence in combination with decreased turbulence intensity in the outer flow. The plug flow further thickens downwards in upper transitional plug flows with increasing clay concentration, whilst the maximum turbulence intensity moves away from the bed and decreases. The upward shift in turbulence production is explained through thickening of the viscous sublayer (Best and Leeder, 1993; Li and Gust, 2000) and the development of an internal shear layer (Baas and Best, 2002), which separates the near-bed region from the plug flow region. Further increasing the clay concentration results in fully suppressed turbulence in quasi-laminar plug flows, apart from minor residual turbulence near the base of the flow within a thin shear layer.

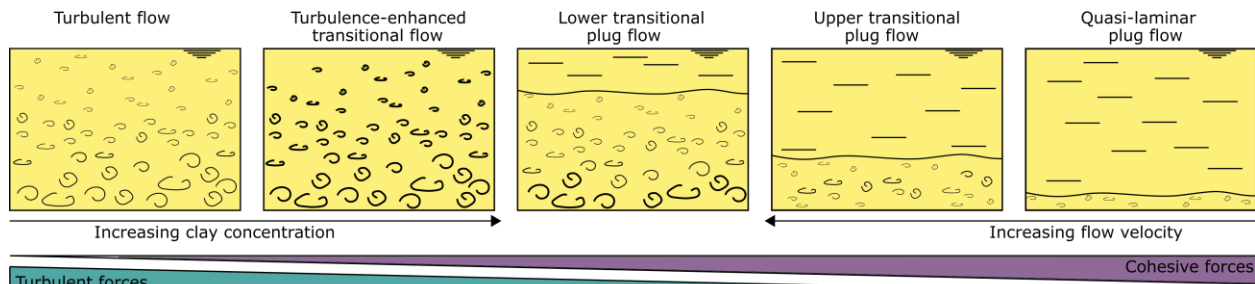


Figure 1. Schematic model of the balance between cohesive and turbulent forces that determines the behaviour of turbulent, transitional, and laminar clay-laden flows, divided into five different phases after the classification scheme of Baas et al. (2009). Modified after Baas et al. (2009).

Flows are naturally non-uniform; here, flow non-uniformity is taken to refer to streamwise changes in depth-averaged velocity. Predicted sediment transport rates, assuming uniform flow, may differ from real-world rates (Wan and Wang, 1994). The effect of clay on streamwise decelerating and accelerating flow is essential for understanding sediment-laden flow dynamics. The formation of bonds between cohesive sediment particles is a time-dependent (thixotropic) process and, therefore, cohesive-sediment laden flows need time to adjust to spatial variations in flow velocity. However, the changing balance between turbulent and cohesive forces in clay-laden flows under non-uniform conditions is poorly understood. Understanding this balance is pivotal, as erosion, transport, and deposition of sediment depend on the magnitude and distribution of flow turbulence (Dorrell et al., 2018). Spatio-temporal increases and decreases in turbulence directly affect the transport capacity and deposition and erosion patterns (Dorrell and Hogg, 2012; Moody et al., 2013).

An increased understanding of the influence of cohesive sediment on non-uniform flow conditions is needed. This paper details experimental results on the flow structure of clay-laden flows, for the first time isolating the effect of non-uniformity on spatial deceleration and acceleration in open-channel flows. We address the following research questions: (1) What are the mean flow and turbulence characteristics of horizontally decelerating and accelerating clay-laden flows? (2) How do non-uniform flows with different suspended clay concentration compare to each other and to uniform clay-laden flows? (3) How much time do decelerating and accelerating flows need to adapt to the changing flow conditions?

## 2 Methodology

Mixtures of pure kaolinite (Imerys Polwhite-E, median particle size  $D_{50} = 9 \mu\text{m}$ , sediment density  $\rho_s = 2600 \text{ kg m}^{-3}$ ) and fresh water were circulated through a hydraulic flume by means of a variable-discharge slurry pump (Fig. 2a). The flume was 10 m long and 0.5 m wide, with a standing water depth,  $h_0$ , of 0.15 m. At the upstream end, the flume contained a turbulence-damping grid to straighten the flow. The flow moved over a flat, smooth floor downstream of the turbulence-damping grid. An inset channel was placed in the flume. It had a 0.2 m wide narrow section and a 2.4 m long tapering section. The inset forced the flow through a narrow to wide transition (decelerating flows) or through a wide to narrow transition (accelerating flows) depending on the flow direction (Fig. 2b). Thus, in contrast to earlier work in non-tapering flumes, this channel design enabled controlled spatial changes in the flow velocity and turbulence to be measured.

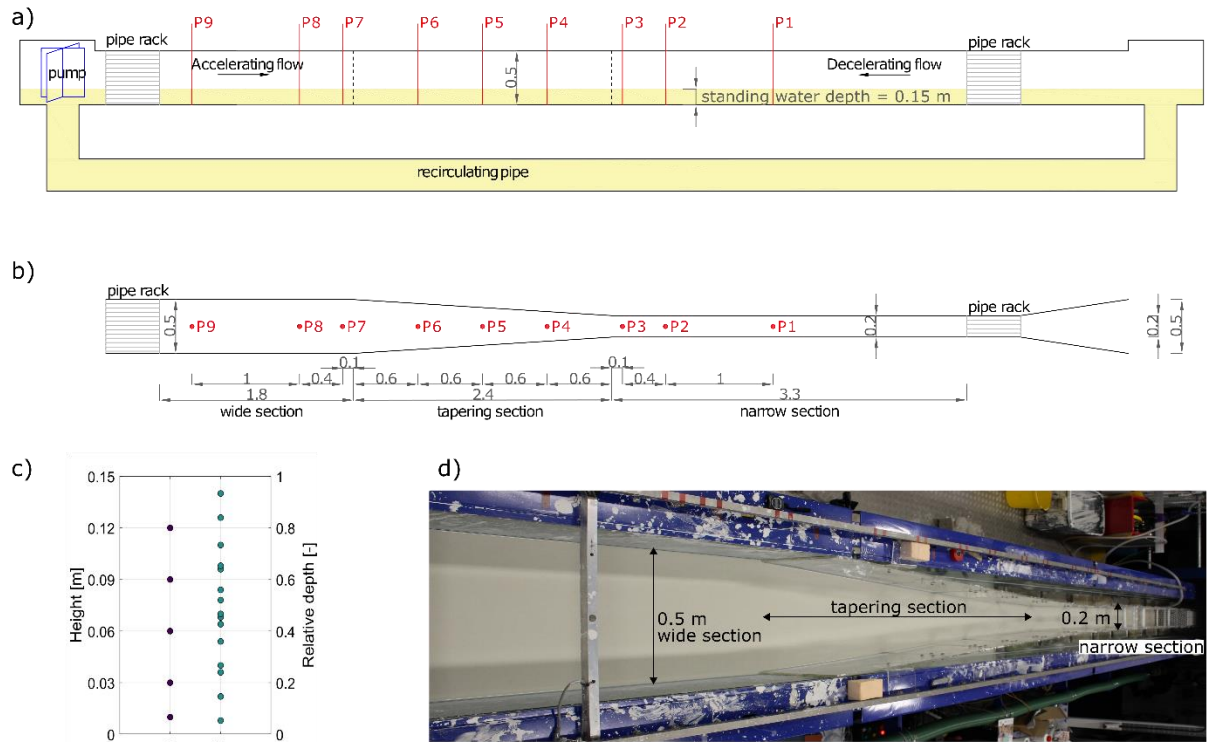


Figure 2. a) Side view of the experimental setup, b) top view of the inset channel, with points P indicating measurement locations, c) velocity (U) and sediment concentration (C) measurement positions above the channel bed; relative depth = height / depth, d) photo of the flume setup. All dimensions in meters.

## 2.1 Experimental conditions

Table 1 shows the range of clay concentrations and flow velocities used; control experiments were conducted with clear water. Clay was soaked in water for a minimum of one day before adding the clay suspension to the flume, to guarantee that no dry clumps remained. The flume ran for 16 to 20 hours to allow the clay-laden flows to reach equilibrium conditions and allow for any deposition of clay before measurements were taken.

Table 1. *Experimental conditions at selected positions in the flume. C = depth-averaged volumetric concentration;  $h_0$  = standing water depth;  $T$  = water temperature;  $\bar{U}$  = depth-averaged velocity;  $Fr$  = Froude number. The labelling of experimental runs is defined using D for decelerating and A for accelerating flows and the value of clay concentration.*

Experimental run	C	$h_0$	T	Measuring point	$\bar{U}$	Fr
	[vol %]	[m]	[°C]		[m/s]	[-]
<i>Decelerating flow</i>						
D1-C0.0	0.00	0.150	16.0	P2	0.69	0.57
				P5	0.52	0.43
				P8	0.33	0.27

D2-C0.0	0.00	0.158	17.6	P2	0.49	0.40
				P5	0.38	0.30
				P8	0.28	0.23
D3-C0.9	0.92	0.150	18.7	P2	0.48	0.39
				P5	0.35	0.29
				P8*	0.28	0.23
D4-C1.5	1.47	0.150	18.0	P2	0.64	0.53
				P5	0.45	0.37
				P8	0.33	0.27
D5-C2.7	2.67	0.150	18.0	P2	0.54	0.45
				P5	0.42	0.35
				P8	0.27	0.22
<i>Accelerating flow</i>						
A1-C0.0	0.00	0.170	17.6	P2	0.45	0.35
				P5	0.26	0.20
				P8	0.16	0.13
A2-C1.4	1.39	0.170	18.0	P2	0.41	0.32
				P5	0.26	0.20
				P8*	0.20	0.17
A3-C1.5	1.54	0.185	18.7	P2	0.43	0.32
				P5	0.27	0.20
				P8*	0.20	0.15
A4-C2.8	2.77	0.180	18.2	P2	0.41	0.31
				P5	0.31	0.23
				P8*	0.20	0.15
* deposition was observed at this location						

## 2.2 Data acquisition

A vertical rack of siphon tubes was used to collect samples at five different heights in the water column and at three locations for the decelerating (P3, P5, P9) and accelerating (P1, P5, P7) flows (Fig. 2b, c). The samples were weighed and dried to determine their volumetric clay concentration. The horizontal flow velocity was measured at nine locations along the flume using Ultrasonic Velocity Profilers facing upstream (Fig. 2b, c) (Takeda, 1991, Best et al., 2001). Five 4 MHz probes were stacked on top of each other with a distance of 14 mm between their centres. The probe array was shifted vertically to three different heights during the experiment to cover the full flow depth, resulting in a total of 15 measurement elevations per location (Fig. 2c). The probes collected velocity data for 500 cycles with a 50 ms delay between probes to avoid measurement interference. Depending on the experimental conditions, these settings resulted in measurement durations of 174 to 330 s at a temporal resolution of 1.5 to 2.9 Hz. Velocity measurements taken at 0.03-0.05 m from the probe head were used in the analysis.

## 2.3 Velocity processing

Artificial noise was removed from the velocity signal by eliminating values three standard deviations away from a temporal moving mean measured over 31 datapoints. Datapoints were

excluded where deposition occurs. The temporal mean flow velocity,  $\bar{U}$ , and its standard deviation,  $RMS(u')$ , were then calculated from the time series of instantaneous velocity data at each measurement height:

$$\bar{U} = \frac{1}{n} \sum_i^n u_i \quad (1)$$

$$RMS(u') = \sqrt{\frac{1}{n} \sum_i^n (u_i - \bar{U})^2} \quad (2)$$

where  $n$  is the number of velocity measurements. A dimensionless measure for turbulence intensity was defined as follows (Baas & Best, 2002):

$$RMS(u')_0 = \frac{RMS(u')}{\bar{U}} \cdot 100 \quad (3)$$

Depth-averaged velocity was calculated by integrating the time-averaged velocities over the depth. The integral was numerically evaluated; velocities were set to zero at the bed and velocities at the water surface were assumed to have the same value as the first measurement position below that level:

$$\bar{\bar{U}} = \frac{1}{h_0} \int_0^{h_0} \bar{U} dz \quad (4)$$

where  $z$  is height above the bed. Depth-averaged turbulence intensity was calculated by integrating the turbulence intensity values over the depth.

$$\overline{RMS(u')_0} = \frac{1}{h_0} \int_0^{h_0} RMS(u')_0 dz \quad (5)$$

Outliers within the processed dataset were excluded as follows. Data was identified as an outlier when either the flow velocity,  $\bar{U}$ , or its standard deviation  $RMS(u')$ , was 40% higher or lower than the median value of the six immediately surrounding measurement points from the nearest upstream and downstream locations. Here, the median was used to avoid weighting from outliers. At the outer locations, P1 and P9, the points within the narrow (P2 and P3) or wide (P7 and P8) section were used to include a sufficient number of measurement points in the determination of the median. Near the bed, larger changes in  $\bar{U}$  and  $RMS(u')$  are likely. Therefore, the lowest measurement elevation was excluded from the outlier analysis. The full measurement location (P1-P9) was deemed invalid if >50% of the data was classified as outliers over the full flow depth. The bed height,  $z_b$ , was defined as the lowest valid measurement elevation. To compare the same elevation within different flows, the flows are plotted against normalized height adjusted to the deposit level.

$$\tilde{z} = (z - z_b)/h_0 \quad (6)$$

### 3 Results

#### 3.1 Clay concentration

The suspended sediment concentrations for the decelerating flows were nearly uniform over the flow depth (Fig. 3), apart from run D3-C0.9, which contained a higher clay concentration at the lowest sampling point within the wide section of the flume. The suspended sediment concentrations for the accelerating flows were non-uniform along the flume, with higher near-bed sediment concentrations, particularly in the wide section of the flume.

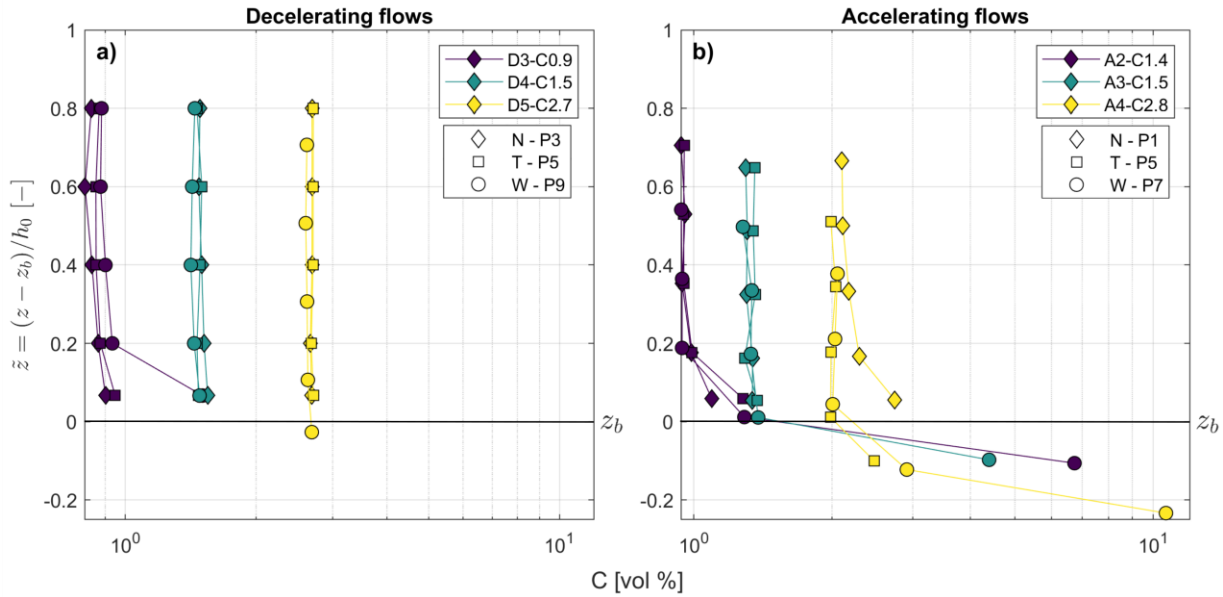


Figure 3. Vertical profiles of volumetric sediment concentration for the a) decelerating and b) accelerating clay-laden flows. N, T and W denote narrow, tapering, and wide sections, respectively.

#### 3.2 Decelerating flows

##### 3.2.1 Clear water flows

Figure 4a shows the time-averaged streamwise velocity profiles ( $\bar{U}$ ) and the depth-averaged velocity magnitudes ( $\bar{\bar{U}}$ ) along the flume for the decelerating clear-water flow D1-C0.0. Upstream, in the narrow section of the flume (P1 to P3; Fig. 2b), the depth-averaged velocity shows that the flow is nearly uniform. The velocity decreases progressively as the width of the flume increases (P4 to P6) and continues to decrease more gradually within the wide section of the flume (P7 to P9). At the end of the flume (P9), uniform conditions are established in the lower half of the flow, but they are not fully established in the upper half. Figure 4b shows the velocities along the flume for the lower-discharge decelerating flow D2-C0.0 (Table 1). The depth-averaged velocities show a comparable pattern to flow D1-C0.0 (Fig. 4a, b).

Figures 4c and 4d show the time-averaged streamwise turbulence intensity profiles ( $RMS(u')_0$ ) and the depth-averaged turbulence intensities ( $\bar{\bar{RMS(u')}}_0$ ) along the flume for D1-C0.0 and D2-C0.0, respectively. The depth-averaged turbulence intensity values of both flows are nearly



uniform in the narrow section (P1 to P3). The turbulence intensities decrease away from the bed in the narrow section (Fig 4c, d). As the velocity decreases in the widening section (P4 to P6), turbulence intensity increases near the bed, while also progressively increasing upwards in the flow downstream. In both flows, this results in an increase in vertical gradient of turbulence intensity within the widening section followed by a decrease in the vertical gradient in the wide section. The depth-averaged turbulence intensity at P9 is 4.0 times higher than at P2 for D1-C0.0 (Fig. 4c) and 3.7 times higher for D2-C0.0 (Fig. 4d), despite the decrease in velocity. Similar increases in turbulence intensity have been observed before (Kironota and Graf, 1995; Qingyang, 2009). Towards the end of the wide section, at P9, the turbulence intensities remain non-uniform, suggesting that the length of the flume is insufficient to establish equilibrium after the widening section.

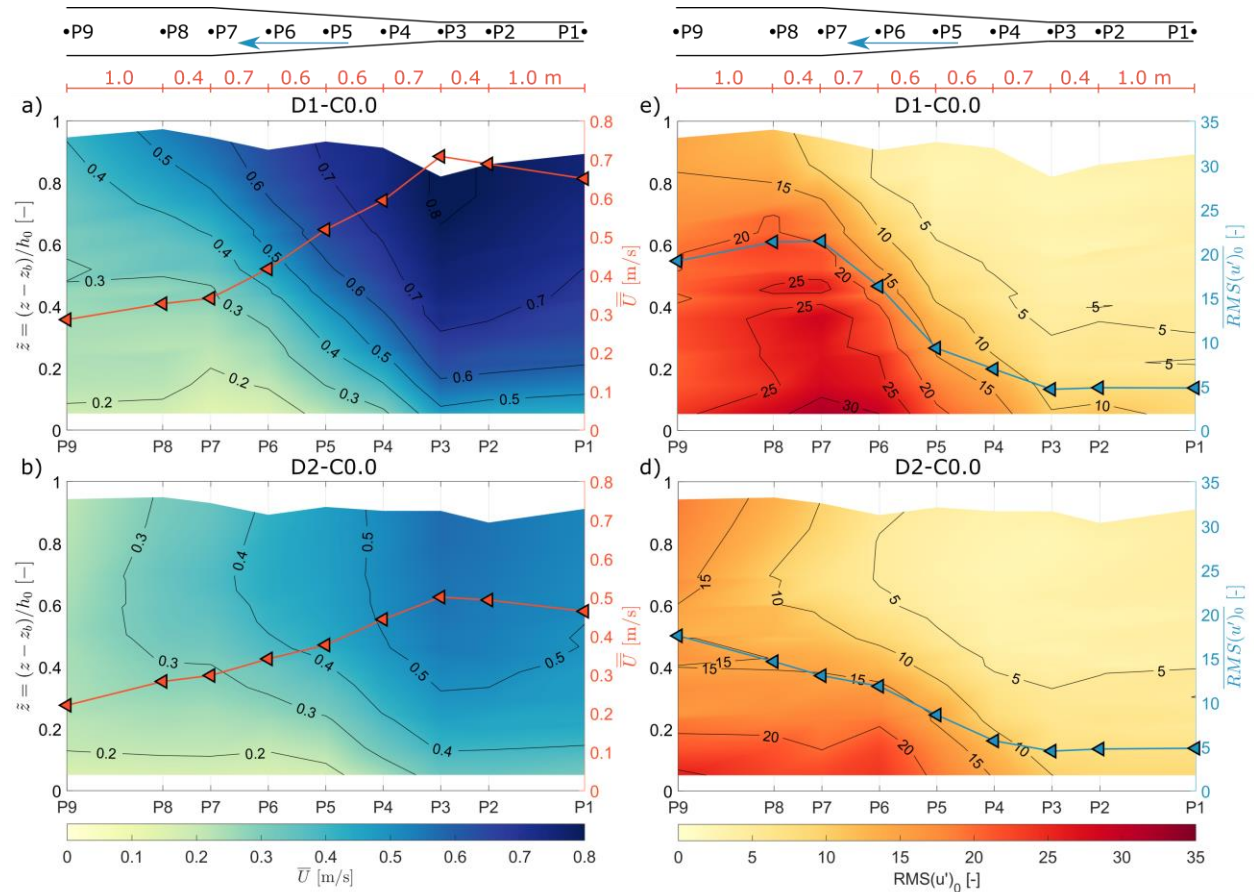


Figure 4. Depth-averaged velocity magnitudes ( $\bar{U}$ ) and time-averaged streamwise velocity profiles ( $\bar{U}$ ) along the flume for the decelerating clear water flows a) D1-C0.0 and b) D2-C0.0. Depth-averaged turbulence intensities ( $RMS(u')_0$ ) and time-averaged streamwise turbulence intensity profiles ( $RMS(u')_0$ ) along the flume for flows c) D1-C0.0 and d) D2-C0.0.

### 3.2.2 Clay-laden flows

Figures 5a, 5b and 5c show the time-averaged streamwise velocity profiles ( $\bar{U}$ ) and the depth-averaged velocity magnitudes ( $\bar{U}$ ) along the flume for the clay-laden decelerating flows D3-C0.9,

D4-C1.5 and D5-C2.7, respectively. Figures 5d, 5e and 5f show the time-averaged streamwise turbulence intensity profiles ( $RMS(u')_0$ ) and the depth-averaged turbulence intensities ( $\overline{RMS(u')_0}$ ) along the flume for the same flows. In the narrow section (P1 to P3), the depth-averaged velocities are nearly uniform for each decelerating clay-laden flow. The depth-averaged velocities for each flow decrease along the widening section similarly, albeit with a slightly higher rate of decrease for flow D4-C1.5. Within the wide section (P7 to P9), the depth-averaged velocities are lowest and nearly uniform. At the downstream end of the flume (P9), near uniform conditions are established in the lower half of the flume, but these are not fully established in the upper half.

The depth-averaged turbulence intensity values are nearly uniform in the narrow section (P1 to P3) (Figs 5d, 5e and 5f); the turbulence intensities decrease away from the bed. As the velocity decreases in the widening section (P4 to P6), the turbulence intensity increases, initially near the bed, and then progressively higher in the flow downstream. This results in an increase in vertical gradient of turbulence intensity in the widening section followed by a decrease in vertical gradient into the wide section. Towards the end of the wide section, at P9, the turbulence intensity shows a steep vertical gradient for flows D3-C0.9 and D4-C1.5. The turbulence intensity for flow D5-C2.7 remains high between P7 and P9. Despite the decrease in velocity, the depth-averaged turbulence intensity at P9 is 3.6 times higher than at P2 for D3-C0.9, 4.3 times higher for D4-C1.5 and 1.8 times higher for D5-C2.7. Towards the end of the wide section, at P9, the turbulence intensities remain non-uniform, suggesting that the length of the flume is insufficient to establish equilibrium after the widening section.

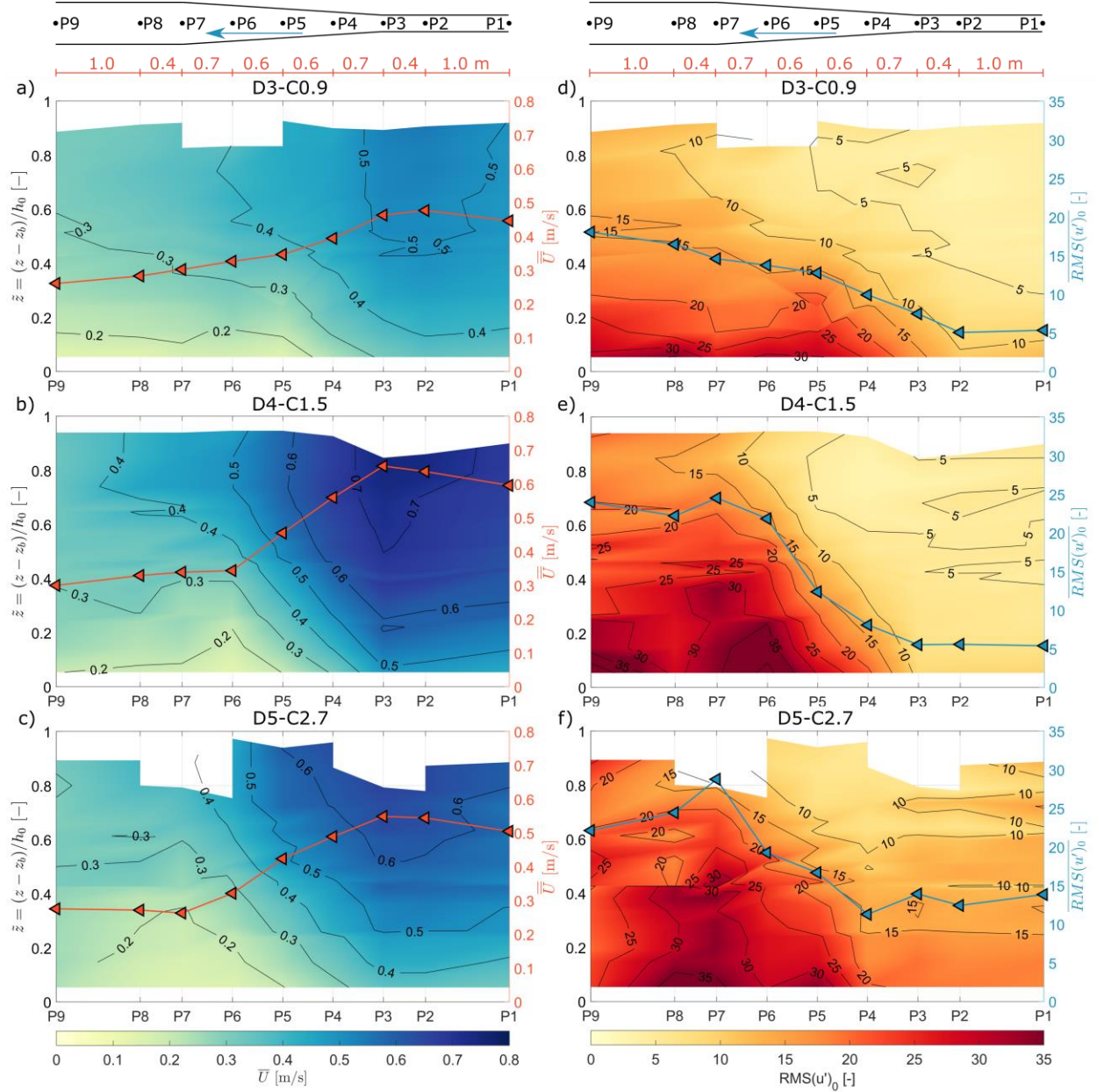


Figure 5. Depth-averaged velocity magnitudes ( $\bar{U}$ ) and time-averaged streamwise velocity profiles ( $\bar{U}$ ) along the flume for the decelerating clay-laden flows a) D3-C0.9, b) D4-C1.5 and c) D5-C2.7. Depth-averaged turbulence intensities ( $RMS(u')_0$ ) and time-averaged streamwise turbulence intensity profiles ( $RMS(u')_0$ ) along the flume for flows d) D3-C0.9, e) D4-C1.5 and f) D5-C2.7.

### 3.3 Accelerating flows

The flow direction was reversed to achieve accelerating conditions, so the flow direction was from left to right, i.e. from P9 to P1 (cf. Fig. 2a and 2b).

### 3.3.1 Clear water flows

Figure 6a shows the time-averaged streamwise velocity profile ( $\bar{U}$ ) and the depth-averaged velocity magnitude ( $\bar{\bar{U}}$ ) along the flume for the accelerating clear-water flow A1-C0.0. Upstream, in the wide section of the flume (P9 to P7; Fig. 2b), the depth-averaged velocity shows that the flow is nearly uniform. The flow accelerates progressively as the width of the flume decreases (P6 to P4) and nearly uniform flow re-establishes within the narrow section (P3 to P1).

Figure 6b shows the time-averaged streamwise turbulence intensity profile ( $RMS(u')_0$ ) and the depth-averaged turbulence intensities ( $\bar{\bar{RMS(u')}}_0$ ) along the flume for flow A1-C0.0. The depth-averaged turbulence intensity values are nearly uniform in the wide section (P9 to P7). The turbulence intensity values decrease as the velocity increases in the narrowing section (P6 to P4) and remain nearly uniform in the narrow section (P3 to P1). The depth-averaged turbulence intensity at P1 is lower by a factor of 0.3 than at P8, despite the increase in velocity. Similar decreases in turbulence intensity have been observed before (Cardoso et al., 1991).

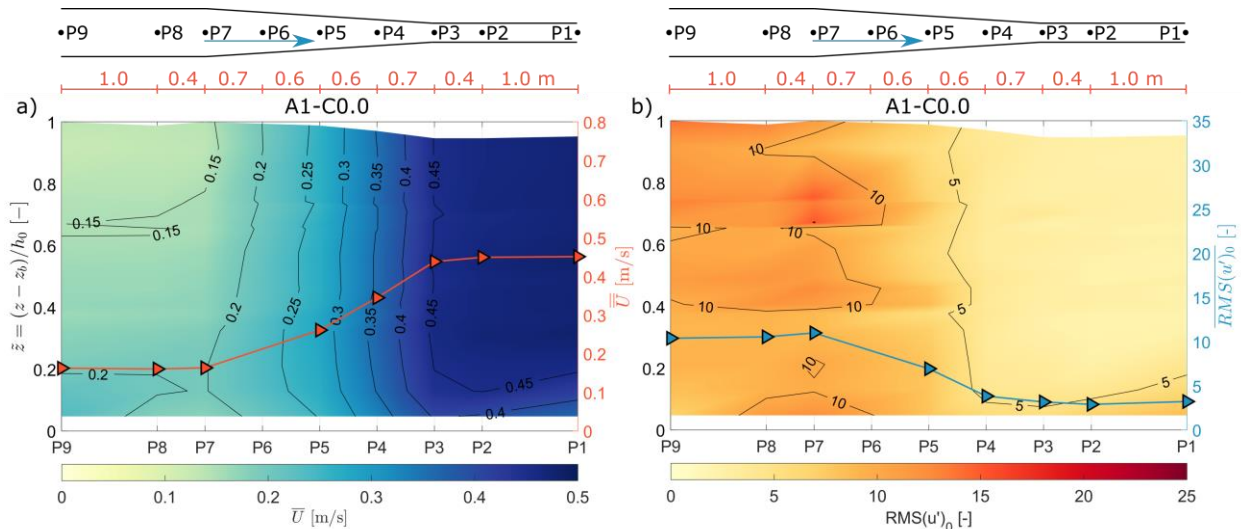


Figure 6. Depth-averaged velocity magnitudes ( $\bar{\bar{U}}$ ) and time-averaged streamwise velocity profiles ( $\bar{U}$ ) along the flume for the accelerating clear water flow a) A1-C0.0. Depth-averaged turbulence intensities ( $\bar{\bar{RMS(u')}}_0$ ) and time-averaged streamwise turbulence intensity profiles ( $RMS(u')_0$ ) along the flume for flow b) A1-C0.0.

### 3.3.2 Clay-laden flows

Figures 7a, 7b and 7c show the time-averaged streamwise velocity profiles ( $\bar{U}$ ) and the depth-averaged velocity magnitudes ( $\bar{\bar{U}}$ ) along the flume for the clay-laden accelerating flows A2-C1.4, A3-C1.5 and A4-C2.8, respectively. Figures 7d, 7e and 7f show the time-averaged streamwise turbulence intensity profiles ( $RMS(u')_0$ ) and the depth-averaged turbulence intensities ( $\bar{\bar{RMS(u')}}_0$ ) along the flume for the same flows. Upstream in the wide section (P9 to P7; fig 2b), the depth-averaged velocity shows that the flow is nearly uniform. The flow accelerates progressively as the width of the flume decreases (P6 to P4) and nearly uniform flow re-establishes within the narrow section (P3 to P1).

308 In the wide section (P9 to P7), where the velocity is low, the depth-averaged turbulence  
309 intensities of all three clay flows are higher than in the narrowing and narrow sections, where the  
310 velocities are higher (Fig. 7d, 7e and 7f). Towards the base of the flow, the turbulence intensity  
311 shows a steep vertical gradient in the wide section, with especially high turbulence intensity  
312 towards the base of flows A2-C1.4 and A3-C1.5. Notably, the turbulence intensity in the bottom  
313 half of the flow at P9 and P8 in the wide section of the flume is lower for flow A4-C2.8 (Fig. 7f)  
314 than for flows A2-C1.4 (Fig 7d) and A3-C1.5 (Fig 7e). The turbulence intensity values are high  
315 around P7 for flow A4-C2.8. The depth-averaged turbulence intensity values for all three flows  
316 decrease as the velocity increases in the narrowing section (P6 to P4) and remain nearly uniform  
317 in the narrow section (P3 to P1). The depth-averaged turbulence intensity at P1 is 0.4 times the  
318 intensity at P8 for A2-C1.4, 0.4 times for A3-C1.5 and 0.8 times for A4-C2.8, despite the  
319 increase in velocity.

320



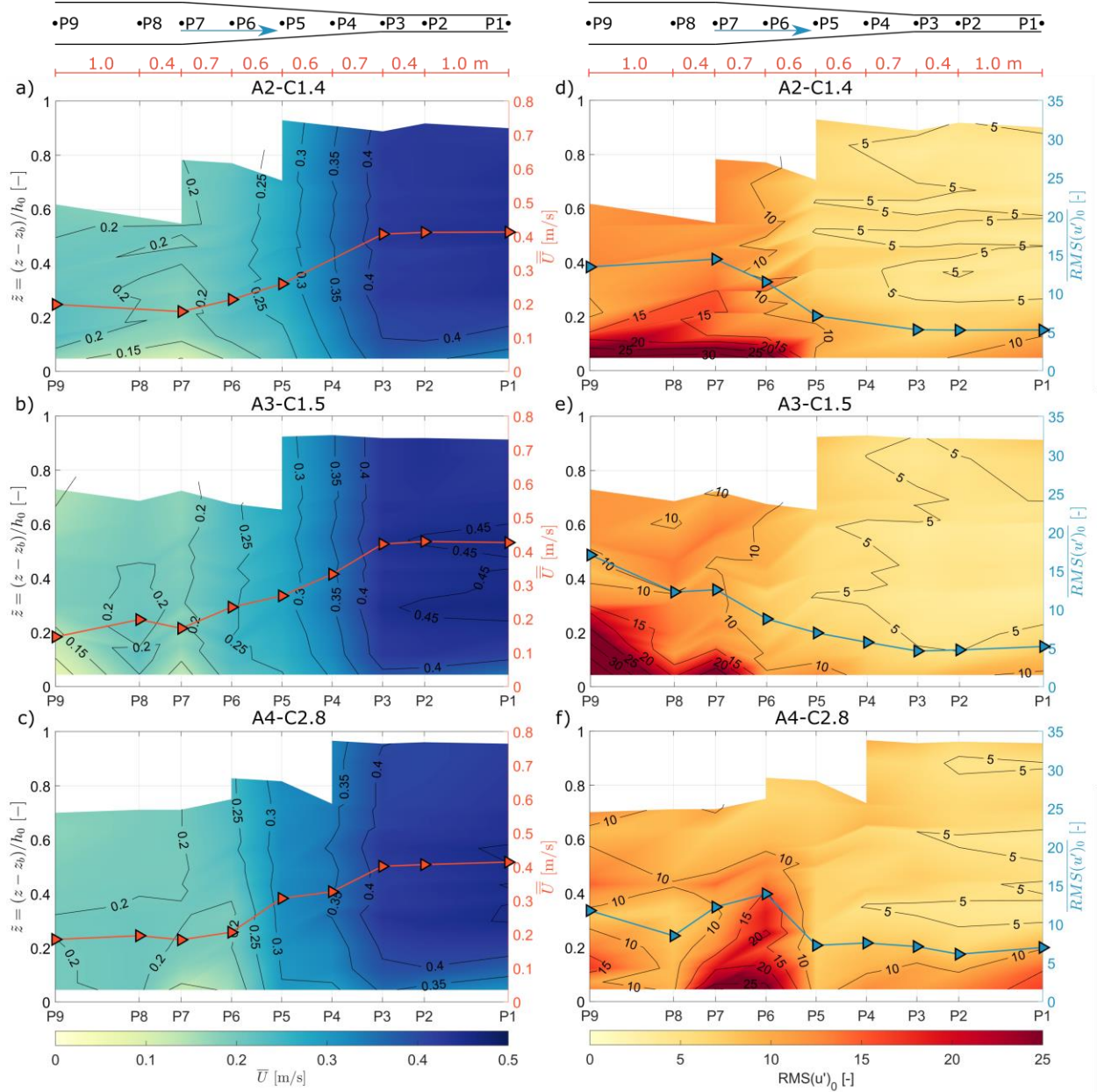


Figure 7. Depth-averaged velocity magnitudes ( $\bar{U}$ ) and time-averaged streamwise velocity profiles ( $\bar{U}$ ) along the flume for the accelerating clay-laden flows a) A2-C1.4, b) A3-C1.5 and c) A4-C2.8. Depth-averaged turbulence intensities ( $RMS(u')_0$ ) and time-averaged streamwise turbulence intensity profiles ( $RMS(u')_0$ ) along the flume for flows d) A2-C1.4, e) A3-C1.5 and f) A4-C2.8.

## 4 Discussion

### 4.1 Flow types

Figures 8a and 8b show the difference in time-averaged streamwise turbulence intensity profiles ( $\Delta RMS(u')_0$ ) and in depth-averaged turbulence intensities ( $\Delta \overline{RMS(u')_0}$ ) along the flume for

decelerating flows D3-C0.9 and D5-C2.7 versus flow D2-C0.0. Upstream, in the narrow section (P1 to P3; Fig. 2b), the turbulence intensity values of flow D3-C0.9 are comparable with the clear-water flow D2-C0.0, i.e., the  $\Delta RMS(u')_0$  values are relatively close to zero. This suggests turbulent flow, unaffected by the presence of the suspended clay. As the flow decelerates in the widening section (P4 to P6), the  $\Delta RMS(u')_0$  values increase to 10 in the lower half of the flow and to 2.5 in the upper half of the flow. This is typical of turbulence-enhanced transitional flow (Baas et al., 2009); under these conditions the presence of the clay is inferred to cause a thickening of the viscous sublayer and the development of an internal shear layer with associated enhancement of turbulence (Best and Leeder, 1993; Li and Gust, 2000; Baas and Best, 2002). In the wide section (P7 to P9), the  $\Delta RMS(u')_0$  values remain above zero in the bottom half of flow D3-C0.9 and they are zero or below zero in the top half of the flow. These negative  $\Delta RMS(u')_0$  values suggest the onset of plug development in flow D3-C0.9, i.e., lower transitional plug flow (Baas et al., 2009). Flows D3-C0.9 and D4-C1.4 show comparable  $\Delta RMS(u')_0$  patterns (Fig. 5d and 5e), such that the same flow types can be identified.

In the narrow section (P1 to P3), the increased clay concentration in flow D5-C2.7 is inferred to cause the observed positive  $\Delta RMS(u')_0$  values. This suggests that flow D5-C2.7 begins as a turbulence-enhanced transitional flow (Fig. 8b; Baas and Best, 2002). The  $\Delta RMS(u')_0$  values progressively increase through the widening section and beyond, suggesting the development of stronger turbulence-enhanced transitional flow (Baas et al., 2009). While the mean velocity profile of flow D5-C2.7 appears reliable, the heterogeneous vertical pattern of  $\Delta RMS(u')_0$  above a relative depth of 0.4 at position P9 (Fig. 8b) may arise from artefacts in the  $RMS(u')$  measurements of this flow. This hinders a reliable inference of flow type at this location, but the decrease in  $\Delta RMS(u')_0$  below the relative depth of 0.4 between P8 and P9 combined with a decrease in  $\Delta RMS(u')_0$  near the top of the flow between P8 and P7 may indicate a change from turbulence-enhanced transitional flow via lower transitional plug flow to upper-transitional plug flow in the wide section (P7 to P9).

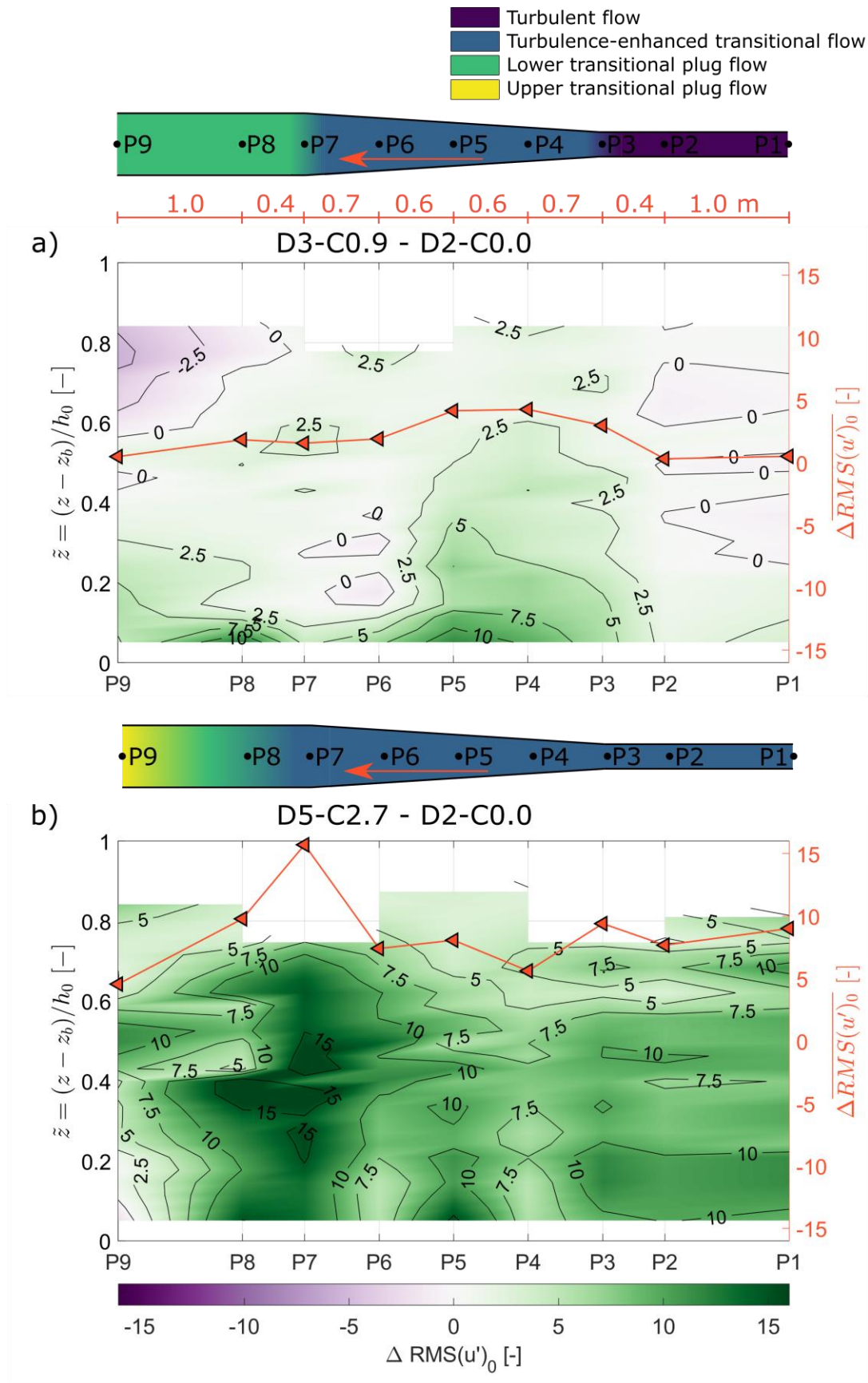




Figure 8. Difference in depth-averaged turbulence intensities ( $\overline{\Delta RMS(u')_0}$ ) and time-averaged streamwise turbulence intensity profiles ( $\Delta RMS(u')_0$ ) along the flume for decelerating flows a) D3-C0.9 minus D2-C0.0 and b) D5-C2.7 minus D2-C0.0.

Figures 9a and 9b show the difference in time-averaged streamwise turbulence intensity profiles ( $\Delta RMS(u')_0$ ) and in depth-averaged turbulence intensities ( $\overline{\Delta RMS(u')_0}$ ) along the flume for accelerating flows A2-C1.4 and A4-C2.8 versus flow A1-C0.0. Upstream, in the wide section and at the start of the narrowing section (P9 to P6),  $\Delta RMS(u')_0$  values are relatively close to zero in the upper half of the flow and increase downwards to 15 in the lower half of flow A2-C1.4. The high near-bed  $\Delta RMS(u')_0$  values, in combination with the low values in the upper half of the flow, are typical of lower transitional plug flow (Baas et al., 2009). As the flow accelerates through the narrowing section (P6 to P4), the near bed  $\Delta RMS(u')_0$  values progressively decrease from 10 to c. 2.5. In the narrow section (P3 to P1), the absolute turbulence intensity values of flow A2-C1.4 are low (Fig. 7d), but the  $\Delta RMS(u')_0$  values are increased to around 2.5. This enhanced turbulence intensity suggests weakly turbulence-enhanced or turbulent flow. Flow A3-C1.5 shows comparable turbulence intensity patterns and values (Fig. 7d and 7e) and similar flow types can be identified.

Upstream, in the wide section (P9 to P8),  $\Delta RMS(u')_0$  values are up to 2.5 in the lower half of the flow and down to -2.5 in the upper half for flow A4-C2.8 (Fig. 9b). This profile suggests upper transitional plug flow, where turbulence enhancement near the bed is lower than for lower transitional plug flows (cf., flow A2-C1.4 in Fig. 9a). Similar to flow A2-C1.4,  $\Delta RMS(u')_0$  values of flow A4-C2.8 between P7 and P6 are relatively close to or below zero in the upper half of the flow and are as high as 15 in the lower half of the flow, suggesting lower transitional plug flow (Fig. 9b). Between P4 and P1, the depth-averaged  $\overline{\Delta RMS(u')_0}$  values are between 2.5 and 5 and vertical  $\Delta RMS(u')_0$  profiles are strictly positive, suggesting turbulence-enhanced transitional flow.

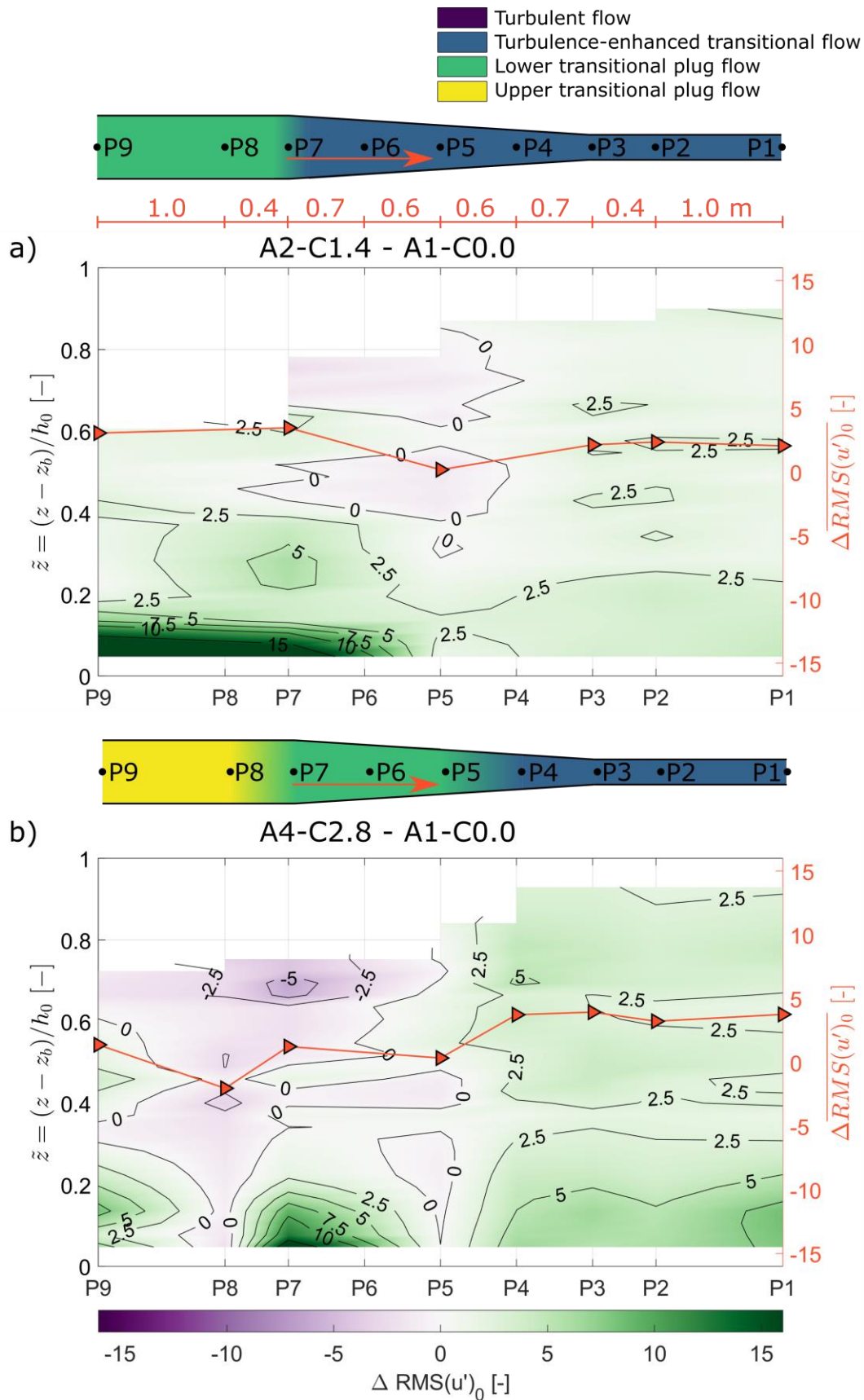


Figure 9. Difference in depth-averaged turbulence intensities ( $\overline{\Delta RMS(u')_0}$ ) and time-averaged streamwise turbulence intensity profiles ( $\Delta RMS(u')_0$ ) along the flume for decelerating flows a) A2-C1.4 minus A1-C0.0 and b) A4-C2.8 minus A1-C0.0.

#### 4.2 Adaptation length scales

The length scales needed by clay flows to adapt to non-uniform conditions can be estimated using the data presented in Fig. 8 and 9. These estimations involve length scales downstream of the start of the widening section for the decelerating flows and the narrowing section of the accelerating flows, as well as in the wide section for the decelerating flows and in the narrow section for the accelerating flows.

As it decelerated at the start of the widening section (P3), flow D3-C0.9 changed from turbulent flow to turbulence-enhanced transitional flow, without a significant adaptation length at this position (Fig. 8a). Throughout the wide section (P7 to P9), the flow adjusted from turbulence-enhanced transitional flow to lower transitional plug flow. Towards the end of the wide section, at P9,  $\Delta RMS(u')_0$  remained non-uniform, suggesting that the length of the flume is insufficient to establish uniform conditions after the widening section (Fig. 8a). Hence, the minimum adaptation length needed to change from turbulence-enhanced flow to lower transitional plug flow was 1.4 m, the full distance between P7 and P9. At the depth-averaged velocity of 0.28 m/s in the wide section, this adaptation length corresponds to a minimum adaptation time of 5.0 s.

Flow D5-C2.7 changed from turbulence-enhanced transitional flow via lower transitional plug flow to upper transitional plug flow in the wide section (P7 to P9), without apparently reaching uniform flow conditions (Fig. 8b). This is equivalent to a minimum adaptation time of 5.2 s at a depth averaged flow velocity of 0.27 m/s through the 1.4-m long wide section. Flow D5-C2.7 started to change from a relatively weak to a stronger turbulence-enhanced transitional flow at position P4, i.e., 0.7 m into the widening section (Fig. 5f), whereas  $\overline{\Delta RMS(u')_0}$  started to increase in flow D2-C0.0 at P3, i.e., at the start of the widening section (Fig. 4d). The maximum adaptation length this high-concentration clay flow needed after starting to experiencing flow widening was therefore 0.7 m. This is equivalent to an adaptation time of 1.4 s at a mean depth-averaged flow velocity of 0.52 m/s between P3 and P4.

Both flow A2-C1.4 and A4-C2.8 established uniform turbulence-enhanced transitional flow at the start of the narrow section, at P3 (Fig. 9). Hence, within the spatial resolution of the experiments, the adaptation length within the narrow section was at or close to zero. Flow A4-C2.8 started to change from upper transitional plug flow to lower transitional plug flow at the start of the narrowing section, at P7. Hence, the change in clay flow type also lacked a significant delay at this location.

Table 2. Adaptation time,  $T$ , and length,  $L$ , scales.

Experimental run	Point(s)	Flow regimes	L	T
			[m]	[s]
<i>Decelerating flow</i>				
D3-C0.9	P3	Turbulent flow to turbulence-enhanced transitional flow	0	0

	P7 to P9	Turbulence-enhanced transitional flow to lower transitional plug flow	$\geq 1.4$	$\geq 5.0$
D5-C2.7	P3 to P4	Weak to strong turbulence-enhanced transitional flow	0.7	1.4
	P7 to P9	Turbulence-enhanced transitional flow to upper transitional plug flow	$\geq 1.4$	$\geq 5.2$
<i>Accelerating flow</i>				
A2-C1.4	P3	Lower transitional plug flow to turbulence-enhanced transitional flow	0	0
A4-C2.8	P7	Upper transitional plug flow to lower transitional plug flow	0	0
	P3	Lower transitional plug flow to turbulence-enhanced transitional flow	0	0

The estimations of adaptation length and time scales show that the decelerating flows generally needed longer to adapt to the imposed non-uniform conditions than the accelerating flows (Table 2). The largest adaptation lengths and times were at the end of the widening section in the decelerating flows, where the flows changed from turbulence-enhanced transitional flow to more cohesive lower and upper transitional plug flows. Whereas, the accelerating flows changed from the more cohesive lower transitional plug flow to turbulence-enhanced flow already within the narrowing section. These differences in adaptation length between the decelerating and accelerating flows can be explained by the fact that establishing cohesive bonds between clay particles, as in the decelerating flows, requires more time than breaking up these bonds, as in the accelerating flows. Furthermore, it appears to take longer to establish a pervasive network of clay bonds, as in the change from turbulence-enhanced transitional flows to lower and upper transitional plug flow at the end of the widening section in the decelerating flows, than to establish a turbulence-enhanced transitional flow from a turbulent flow by reducing the flow velocity in low-concentration clay flows (e.g., Fig. 8a).

Length and time scales of flow adaptation to changing environments are reflected in the depositional product (Dorrell and Hogg, 2012). This study demonstrates that for mud-rich flows such scales differ between decelerating and accelerating regimes, due to the time required to form and break down the cohesive bonds between particles, whose presence affects the flow dynamics. Depending on the boundary conditions, this difference likely impacts sedimentation patterns within muddy rivers. For example, after a sediment supply increase following wild-fire related erosion (Renau et al., 2007; Sankey et al., 2017; Nyman et al., 2019), flow deceleration can occur following for example, a reduction in bed slope or widening of the river channel. The flow deceleration reduces the turbulent forces in the flow and allows the establishment of cohesive bonds between clay particles. The adaptation to stronger turbulence attenuated clay flow types requires time due to the formation of clay bonds and consequently, the deposits associated with the clay flow type form over the adaptation length scale downstream of the location of flow deceleration. In an industrial setting such as downstream of dam flushing or venting events flow acceleration can occur (Antoine et al., 2020), increasing the turbulent forces within the flow, which has the potential to break up bonds between clay particles. This study shows that the adaptation of the clay flow type to a stronger turbulent flow occurs more rapidly and consequently the associated deposits with clay flow type occur near the location of

acceleration. Additionally, the different adaptation length and time scales are of particular relevance in interpreting the shape of submarine deposits, such as unconfined submarine lobes (Spychala et al., 2017) and hybrid event beds deposited around diapires (Davis et al., 2009; Patacci et al., 2014). It is anticipated that the depositional record of decelerating flows reflects the time scales required to form interparticle bonds, delaying the depositional response to the associated changes in flow conditions. For accelerating flows it is anticipated that changes in deposit properties associated with bond breakage occur more rapidly, such that they are more closely associated with the areas where acceleration occurs.

## 5 Conclusions

This research investigated the influence of suspended cohesive clay on changing flow dynamics under non-uniform flow conditions, using decelerating and accelerating open-channel flows in a recirculating flume. These flows may evolve through different clay flow types with different associated degrees of turbulence enhancement and attenuation depending on the clay concentration and whether the flows decelerate or accelerate. Decelerating flows have a longer adaptation time than accelerating flows, as establishing cohesive bonds between clay particles requires more time than breaking the clay bonds. This hysteresis is more pronounced for higher-concentration flows that change from the turbulence-enhanced transitional flow type to the lower and upper transitional plug flow types than for lower-concentration decelerating flows that change from the turbulent flow type to the turbulence-enhanced transitional flow type. Differences in adaptation time likely influence the distribution and character of deposit within sedimentary environments. The associated deposits with clay flow type of decelerating flows are likely spread over a larger distance than of accelerating flow due to the elongated adaptation time of decelerating flows.

## Acknowledgements

This work was carried out as part of a PhD studentship, part funded through the Turbidites Research Group, University of Leeds and part funded through the University of Hull. Bangor University is thanked for loan of UVP equipment for the duration of the experiments. RMD is grateful for funding from NERC NE/S014535/1. Participation of RF in this study has been possible thanks to The Leverhulme Trust, Leverhulme Early Career Researcher Fellowship (grant ECF-2020-679) and the European Research Council under the European Union's Horizon 2020 research and innovation program (grant 725955).

## Data Availability Statement

The data collected during the physical experiments in preparation for this research is available at <https://doi.org/10.5281/zenodo.6642324> (de Vet et al., 2022).

## References

Ackers, J., Butler, D., Leggett, D., & May, R. (2001), Designing sewers to control sediment problems. *Urban Drainage Modeling*, 818-823. doi: 10.1061/40583(275)77

Antoine, G., Camenen, B., Jodeau, M., Nemery, J. & Esteves, M. (2020), Downstream erosion and deposition dynamics of fine suspended sediments due to dam flushing. *Journal of Hydrology*, 585. doi: 10.1016/j.jhydrol.2020.124763

Baas, J.H., & Best, J.L. (2002), Turbulence modulation in clay-rich sediment-laden flows and some implications for sediment deposition. *Journal of Sedimentary Research*, 72(3), 336-340. doi: 10.1306/120601720336

Baas, J.H., Best, J.L., Peakall, J., & Wang, M. (2009), A phase diagram for turbulent, transitional, and laminar clay suspension flows. *Journal of Sedimentary Research*, 79(4), 162-183. doi: 10.2110/jsr.2009.025

Bagnold, R.A. (1954), Experiments on a gravity-free dispersion of large, solid spheres in a Newtonian fluid under shear. *Proceedings of the Royal Society of London. Series A. Mathematical and Physical Sciences*, 225(1160), 49-63. doi:10.1098/rspa.1954.0186

Barbero, R., Abatzoglou, J.T., Larkin, N.K., Kolden, C.A., & Stocks, B. (2015), Climate change presents increased potential for very large fires in the contiguous United States. *International Journal of Wildland Fire*, 24(7), 892-899. doi: 10.1071/WF15083

Best, J.L. (1988), Sediment transport and bed morphology at river channel confluences. *Sedimentology*, 35(3), 481-498. doi: 10.1111/j.1365-3091.1988.tb00999.x

Best, J.L., & Leeder, M.R. (1993), Drag reduction in turbulent muddy seawater flows and some sedimentary consequences. *Sedimentology*, 40(6), 1129-1137. doi: 10.1111/j.1365-3091.1993.tb01383.x

Best, J., Bennet, S., Bridge, J., & Leeder, M.R., (1997), Turbulence modulation and particle velocities over flat sand beds at low transport rates. *Journal of Hydraulic Engineering*, 123(12), 1118-1129. doi: 10.1061/(ASCE)0733-9429(1997)123:12(1118)

Best, J.L., Kirkbridge, A.D., & Peakall, J., (2001), Mean flow and turbulence structure of sediment-laden gravity currents: new insights using ultrasonic Doppler velocity profiling, in McCaffrey, W.D., Kneller, B.C., & Peakall, J., eds., *Particulate Gravity Currents*, *International Association of Sedimentologists, Special Publication*, 31, 159-172. doi: 10.1002/9781444304275.ch12

Bilal, A., Xie, Q., & Zhai, Y., (2020), Flow, Sediment, and Morpho-Dynamics of River Confluence in Tidal and Non-Tidal Environments. *Journal of Marine Science and Engineering*, 8(8), 591. doi: 10.3390/jmse8080591

Brenda, L., & Dunne, T., (1997), Stochastic forcing of sediment supply to channel networks from landsliding and debris flow. *Water Resources Research*, 33(12), 2849-2863. doi: 10.1029/97WR02388

- Cardoso, A.H., Graf, W.H., & Gust, G., (1991), Steady gradually accelerating flow in a smooth open channel. *Journal of Hydraulic Research*, 29(4), 525-543. doi: 10.1080/00221689109498972
- Davis, C., Haughton, P., McCaffrey, W., Scott, E., Hogg, N., & Kitching, D., (2009), Character and distribution of hybrid sediment gravity flow deposits from the outer Forties Fan, Paleocene Central North Sea, UKCS. *Marine and Petroleum Geology*, 26(10), 1919-1939. doi: 10.1016/j.marpetgeo.2009.02.015
- Dorrell, R.M., & Hogg, A.J. (2012), Length and time scales of response of sediment suspension to changing flow conditions. *Journal of Hydraulic Engineering*, 138(5), 430-439. doi: 10.1061/(ASCE)HY.1943-7900.0000532
- Dorrell, R.M., Amy, L.A., Peakall, J., & McCaffrey, W.D. (2018), Particle size distribution controls the threshold between net sediment erosion and deposition in suspended load dominated flows. *Geophysical Research Letters*, 45(3), 1443–1452. doi: 10.1002/2017GL076489
- Geertsema, M., Clague, J.J., Schwab, J.W., & Evans, S.G. (2006), An overview of recent large catastrophic landslides in northern British Colombia, Canada. *Engineering Geology*, 83(1-3), 120–143. doi: 10.1016/j.enggeo.2005.06.028
- Kironoto, B.A., & Graf, W.H. (1995), Turbulence characteristics in rough non-uniform open-channel flow. *Proceedings of the institute of civil engineers water maritime and energy*, 112(4), 336-348. doi: 10.1680/iwtme.1995.28114
- Li, M.Z., & Gust, G. (2000), Boundary layer dynamics and drag reduction in flows of high cohesive sediment suspensions. *Sedimentology*, 47(1), 71-86. doi: 10.1046/j.1365-3091.2000.00277.x
- Mehta, A. J., McAnally Jr, W. H., Hayter, E. J., Teeter, A. M., Schoellhamer, D., Heltzel, S. B., & Carey, W. P. (1989), Cohesive sediment transport. II: Application. *Journal of Hydraulic Engineering*, 115(8), 1094-1112. doi: 10.1061/(ASCE)0733-9429(1989)115:8(1094)
- Moody, J. A., Shakesby, R. A., Robichaud, P. R., Cannon, S. H., & Martin, D. A. (2013), Current research issues related to post-wildfire runoff and erosion processes. *Earth-Science Reviews*, 122, 10-37. doi: 10.1016/j.earscirev.2013.03.004
- Murphy, S.F., Writer, J.H., McClesley, R.B., & Martin, D.A. (2015), The role of precipitation type, intensity, and spatial distribution in source water quality after wildfire. *Environmental Research Letters*, 10(8). doi: 10.1088/1748-9326/10/8/084007
- Nezu, I., & Nakagawa, H. (1993), *Turbulence in Open-Channel Flows*. Delft Hydraulics, International Association for Hydraulic Research, Monograph.

- Niman, P., Box, W.A.C., Stout, J.C., Sheridan, G.J., Keestra, S.D., Lane, P.N.J., & Langhans, C. (2019), Debris-flow-dominated sediment transport through a channel network after wildfire. *Earth Surfaces Processes and Landforms*, 45(5), 115-1167. doi: 10.1002/esp.4785
- Van Olphen, H. (1977), *An introduction to Clay Colloid Chemistry*. 2<sup>nd</sup> Edition: London, John Wiley & Sons.
- Patacci, M., Haughton, P.D.W., & McCaffrey, W.D. (2014), Rheological Complexity In Sediment Gravity Flows To Decelerate Against A Confining Slope, Braux, SE France. *Journal of Sedimentary Research*, 84(4), 270-277. doi: 10.2110/jsr.2014.26
- Partheniades, E. (1965). Erosion and deposition of cohesive soils. *Journal of the Hydraulics Division*, 91(1), 105-139. doi: 10.1061/JYCEAJ.0001165
- Partheniades, E. (2009), *Cohesive sediment in open channels*. Butterworth-Heinemann, Burlington (MA)
- Qingyang, S. (2009), Velocity distribution and wake-law in gradually decelerating flows. *Journal of Hydraulic Research*, 47(2), 177-184. doi: 10.3826/jhr.2009.3254
- Reneau, S.L., Katzman, D., Kuyumjian, G.A., Lavine, A., & Malmon, D.V. (2007), Sediment delivery after a wildfire. *Geology*, 35(2), 151-154. doi: 10.1130/G23288A.1
- Rengers, F.K., McGuire, L.A., Oakley, N.S., Kean, J.W., Staley, D.M., & Tang, H. (2020), Landslides after wildfire: initiation, magnitude, and mobility. *Landslides*, 17, 2631-2641. doi: 10.1007/s10346-020-01506-3
- Sankey, J.B., Kreitler, J., Hawbaker, T.J., McVay, J.L., Miller, M.E., Mueller, E.R., Vaillant, N.M., Lowe, S.E., & Sankey, T.T. (2017), Climate, wildfire, and erosion ensemble foretells more sediment in western USA watersheds. *Geophysical Research Letters*, 44(17), 8884-8892. doi: 10.1002/2017GL073979
- Smith, H.G., Sheridan, G.J., Lane, P.N.J., Nyman, P., & Haydon, S. (2011), Wildfire effects on water quality in forest catchments: A review with implications for water supply. *Journal of Hydrology*, 396(1-2), 170-192. doi: 10.1016/j.jhydrol.2010.10.043
- Spychala, Y.T., Hodgson, D.M., Prelat, A., Kane, I.A., Flint, S.S., & Mountney, N.P. (2017), Frontal and Lateral Submarine Lobe Fringes: Comparing Sedimentary Facies, Architecture and Flow Processes. *Journal of Sedimentary Research*, 87(1), 75-96. doi: 10.2110/jsr.2017.2
- Swanson, F.J. (1981), Fire and geomorphic processes: in Mooney, H.A., et al., eds., *Fire Regimes and Ecosystem Properties*: U.S. Department of Agriculture Forest Service General Technical Report WO-26, 401-444
- Takeda, Y. (1991), Development of an ultrasound velocity profile monitor. *Nuclear Engineering and Design*, 126(2), 277-284. doi: 10.1016/0029-5493(91)90117-Z



Talling, P.J., Masson, D.G., Sumner, E.J., & Malgesini, G. (2012), Subaqueous sediment density flows: Depositional processes and deposit types. *Sedimentology*, 59(7), 1937-2003. doi: 10.1111/j.1365-3091.2012.01353.x

Wan, Z., & Wang, Z. (1994), *Hyperconcentrated flow*. CRC Press.

Wang, Z., & Larsen, P. (1994), Turbulence structure of flows of water and clay suspensions with bedload. *Journal of Hydraulic Engineering*, 120(5), 577-600. doi: 10.1061/(ASCE)0733-9429(1994)120:5(577)

Whitehouse, R. J. S., Soulsby, R. L., Roberts, W., & Mitchener, H. J. (2000). *Dynamics of estuarine muds*. Technical Report. Thomas Telford.

Winterwerp, J.C. & van Kesteren, W.G.M. (2004), *Introduction to the Physics of Cohesive Sediment in the Marine Environment*. Oxford, U.K, Elsevier, Developments in Sedimentology 46.